KU LEUVEN

FACULTY OF PSYCHOLOGY AND

EDUCATIONAL SCIENCES

ADAPTIVE REWIRING ON COUPLED LOGISTIC MAPS WITH HETEROGENEOUS PARAMETERS

Master's thesis submitted for the degree
of Master of Science in Master of
Psychology: Theory and Research by
MohammadHossein Manuel Haqiqatkhah

Supervisor: Professor Cees van Leeuwen

2019-2020

KU LEUVEN

FACULTY OF PSYCHOLOGY AND

EDUCATIONAL SCIENCES

ADAPTIVE REWIRING ON COUPLED LOGISTIC MAPS WITH HETEROGENEOUS PARAMETERS

Master's thesis submitted for the degree
of Master of Science in Master of
Psychology: Theory and Research by
MohammadHossein Manuel Haqiqatkhah

Supervisor: Professor Cees van Leeuwen

2019-2020

Summary

Adaptive rewiring is the driving force of brain plasticity to form modular, small-world connectivity structure. Highly simplified models for adaptive rewiring represent the dynamic activity of neural masses by coupled logistic maps. Such models have thus far used uniform parametrizations, preventing any cognitive functionality. In order to enable cognitive functions, adaptive rewiring has to be robust to non-uniformity of parameters. Moreover, it should enable function-specific structures to emerge from such parameterization.

Coupled logistic maps are characterized by two parameters, namely turbulence (denoted by α), controlling the range of node activation and coupling strength (denoted by $\mathcal{E}$) between nodes. We study five parameterization conditions of an adaptively rewiring coupled map networks. A baseline (BL) condition with uniform values for α and $\mathcal{E}$ is compared with four conditions in which either α or $\mathcal{E}$ of a subset (viz., minority subgraph) deviates from the remaining units (majority subgraph). These conditions are called: under-turbulent (UT) or over-turbulent (OT), according to α; and under-coupled (UC) or over-coupled (OC), according to $\mathcal{E}$. For each condition, 10 model instantiations are run for 20 million discrete updates and undergo one million adaptive rewiring steps. To describe the evolution of model network structure, the clustering coefficient, average path length, small-worldness, modularity, degree assortativity, and edge density are calculated, both for the whole network and its minority and majority subgraphs separately. The rich club coefficient is calculated for the final state of the network. Different conditions are compared by representing networks as multivariate distributions of local network statistics. Aggregate scores of within- and between-condition contrast are defined to measure dissimilarity amongst conditions. The degree to which conditions diverge is evaluated statistically. The results show adaptive rewiring to improve all measures substantially (except for average path length), such that highly modular, small-world network structures evolve from random initial conditions, while the structures evolving in different conditions show considerable differentiation.

This study offers computational support for robustness of adaptive rewiring algorithm under symmetry-breaking conditions regarding the dynamic evolution of properties characteristic to brain networks. Furthermore, function-specific structures and behaviors emerge from such deviations, implying that functional and structural differentiation can be used to identify functional components in a network, upholding the use of structural and functional connectivity measures in neuroimaging.

Keywords: evolving neural networks, structural plasticity, neural oscillators, dynamical systems, complexity

Acknowledgement

I would like to humbly bestow this thesis Professor Simon LeVay, whose influential work on neuroscience of human sexuality had a key role in the drastic change in my academic life; from Telecommunication Engineering and Artificial Intelligence to Psychology. His research on hardwired networks of "The Sexual Brain"—and the role of complex interaction of hormones, genes, and the environment in molding one's gender-related traits and sexual orientation—inspired me to choose my thesis on computational modeling of brain plasticity.

Furthermore, this dissertation is dedicated to my lovely, supportive parents—especially my mother, who never let me give up during this master's program in Psychology—and to Hessamoddin Khorram, who, albeit being physically far, far away, virtually lived with me all along these years; the *brother not given birth by my mother but by the world*, without whose support I would have never reached this far.

Lastly, I would like to sincerely thank my supervisor Professor Cees van Leeuwen for letting me flourish as a family member of his wonderful group—and to learn from his knowledge, wisdom, and manners.

Clarification of the Student's Approach and Contribution to the Thesis

This study investigated the effect of non-uniform parameterizations on the evolution via adaptive rewiring of small-world networks in random networks of coupled logistic maps. I conducted this study as work for my thesis within the Masters' program in Psychology (Theory and Research track) at the Faculty of Psychology and Educational Sciences, KU Leuven. Over two years, I worked under supervision of Professor Cees van Leeuwen, the head of the Perceptual Dynamic Lab (part of the Brain and Cognition Research Unit), who had assigned this project to me. Throughout this project, I had the benefit of close contact with the supervisor and his valuable feedback, as well as from feedback and insights provided by a post-doc in the lab, Dr. Ilias Rentzeperis. The writing underwent multiple revisions by the supervisor, mostly relating to structure of the text and scientific prose.

The study was based upon two strands of literature, one on adaptive rewiring and dynamic systems, and the other concerning methodological matters, mainly revolving around graph theory and its applications. The former resources were provided by the supervisor, and the latter by myself.

The project was principally a modeling study. The software was written exclusively in R programming language. All the steps of writing the scripts for modeling, analysis, and reporting, and further adaptation of the codes for parallel computing and subsequent execution on the High-Performance Computing (HPC) clusters of the Flanders Supercomputer Center (VSC) was performed by myself. On some occasions, the code was debugged with the help of the supervisor.

In line with the values and standards of Open Science, I made all scripts available on the project's repository on GitHub (https://github.com/psyguy/KUL-MPsy-Thesis) and all the results can be fully reproduced using the scripts. Since this study required massive, computationally costly simulations to generate models, all model files (500 files amounting to 101 GB of data, produced on HPC clusters) are made publicly available on a repository at the Open Science Framework (https://osf.io/625d8/). The OSF repository also contains additional plots and visualizations not included in this manuscript.

Table of Contents

Introduction

Brain network architecture is shaped dynamically through structural plasticity (Butz et al., 2009). Structural plasticity encompasses a variety of mechanisms, all of which incorporate the *functional connectivity* between network components, i.e. their mutual statistical dependencies in neural activity (Avena-Koenigsberger et al., 2018; Rubinov et al., 2009). The role of functional connectivity in driving structural plasticity is a common principle that has become known as *adaptive rewiring* (Gong & van Leeuwen, 2003, 2004; Papadopoulos et al., 2017). Adaptive rewiring implements the Hebbian principle of "what fires together, wires together" at the level of network dynamics (Hebb, 1949).

Adaptive rewiring can be modeled in dynamical systems, in which the network components may represent units at the scale of single neurons (Bi & Poo, 2001) or neural masses (Breakspear et al., 2003). In the latter case, the activity may be abstractly described based on a chaotic oscillator, for instance the one governed by the attractor in Figure S1A in the supplementary materials. Dimensional reduction via Poincaré section yields the relationship in Figure S1B that can approximately be described, minus the noise, by a logistic map (Figure S1C). Thus, the logistic map is the simplest possible abstract representation of neural mass activity. Logistic maps are known to exhibit universal dynamical properties (van Strien, 1987).

The logistic map is of the form shown in Equation 1, in which x is a continuous variable in the range <-1,1> which is updated in discrete time t, and α is the *turbulence parameter*. For certain regimes of α, the behavior of the logistic map converges to one or more limit-cycle attractors, but otherwise it exhibits chaotic behavior. In these regimes, logistic maps produce deterministic bounded time series that, indeed, qualitatively resemble the oscillations of neural mass activity (see Figure S1).

$$x_{t+1} = 1 - \alpha x_t^2 \quad (1)$$

Whereas the logistic map could be considered as an abstract representation of neural mass activity, systems of coupled neural mass oscillators may be represented by coupled logistic maps. Because of the universal dynamics of logistic maps, networks of such simple maps may capture generic properties of interacting nonlinear systems (Kaneko, 1992). The logistic maps are coupled according to Equation 2. Through the effect of the neighbors, the map activity of Figure S1C regains a noisy appearance more in line with Figure S1B. In matrix notation, for a network with |V| nodes, the activity of nodes at time $t + 1$ is calculated via Equation 2.

$$X_{t+1} = (1 - X_t\, \alpha^T\, X_t) \odot [1 - \mathcal{E} + (M_t \mathcal{E}) \oslash (M_t\, J_{|\mathrm{V}|,1})] \qquad (2)$$

In this equation, symbols $\odot$ and $\oslash$ respectively denote Hadamard (i.e., element-wise) multiplication and division. The right-hand side of Equation 2 constitutes the vector form of the logistic map, in which α is the vector of turbulence parameters and X_t is the vector of node's activities at time t. The map is Hadamard-multiplied by a coupling term. In the coupling term, $\mathcal{E}$ is the vector of coupling strengths, M_t is the connectivity matrix at time t, and $J_{|\mathrm{V}|,1}$ denotes a vertical unit vector of size |V|. In the coupling term, $M_t \mathcal{E}$ is Hadamard-divided by $M_t\, J_{|\mathrm{V}|,1}$, normalizing the former by the sum of the weights of the edges connected to each node. For binary networks, the term in the denominator counts the number of connections for each node. We consider only binary graphs for convenience. For adaptive rewiring in weighted networks, see Hellrigel, Jarman, and van Leeuwen (2019).

Based on the network activity as defined by Equation 2, adaptive rewiring takes the following form: after several updates to the network activity, a rewiring step is made. At each rewiring step, the connections of a random node are optimized as the node is disconnected from the neighbor most dissimilar in activity and is connected to the most similar nodes to which it was not connected before. The dissimilarity of two nodes at a given time is defined as the absolute value of the difference in the value of their activities. Note that although

rewiring steps are local, the most dissimilar unconnected node is obtained through a global search. For algorithms using local, or rather, regional information for this purpose, see Jarman et al. (2017) and Jarman et al. (2014).

According to the adaptive rewiring principle, network structure evolves over time from random to complex architectures, showing the characteristics of small world, modularity, and the rich club effect (Gong & van Leeuwen, 2003, 2004; Hellrigel et al., 2019; Rubinov et al., 2009). Hence, at least according to these global structural characteristics, adaptively rewiring networks evolve brain-like structures, as small worldness (Sporns & Zwi, 2004), modularity (Meunier et al., 2010) and the rich club effect (van den Heuvel & Sporns, 2011) are characteristics of large-scale brain networks. Adaptive rewiring may thus be considered to capture, in a highly simplified form, the common principle of structural plasticity mechanisms in the brain.

All modeling studies of adaptive rewiring so far have, for simplicity, assumed the coupling strength and turbulence to be uniform across the system. This assumption severely reduces the cognitive functionality of such models. In earlier logistic map network studies using fixed architectures, these parameters have been varied locally to represent perceptual and memory functions. In a network model to model perceptual organization (van Leeuwen et al., 1997), a sensory input function was realized by modulation of the turbulence parameters of the local oscillators. Presence of sensory input brought these parameters down to values imposing a more stable regime on the oscillators. As a result, connected units receiving similar inputs showed a synchronization bias, leading to perceptual grouping preferences. In a memory model (van Leeuwen & Raffone, 2001), connectivity parameter values were locally incremented to represent the presence of a memory trace. This, too, established synchronization biases, leading to spontaneous pattern rehearsals and subsequent relearning of dynamic memory traces.

When networks having cognitive functions are to evolve brain-like structures through adaptive rewiring, adaptive rewiring must be robust to non-uniform parameter values. We will explore the effect of non-uniform turbulence and coupling parameters on adaptive rewiring of coupled logistic maps. In particular, we will compare networks of coupled logistic maps with uniform parameters with those that have a subset of the turbulence and coupling parameters deviate from the majority value. We study the effect of non-uniform parameters on network evolution and final network structure.

In what follows, the method section describes details of the composition and initialization of the models; the rewiring algorithm; and the qualitative and quantitative measures of network structures used to describe, characterize, and compare models. In the results section, we describe our findings, mainly that non-uniformity of parameters is shown not to interfere with the evolution of brain-like structure while giving rise to distinguishable network structures suitable for cognitive functions. A discussion ends the paper.

Method

Description of networks

An undirected, binary graph (or network) *G* is a set of 3-tuples $g = (v_i, v_j, e_{ij})$ of vertices (or nodes) v_i and v_j and an edge (or connection) e_{ij} between them. The connection e_{ij} can assume values of $\{0,1\}$. This set is called adjacency list, wherein, conventionally, zero valued elements are omitted. We assume no self-connection, i.e. $e_{ii} = 0$. The set of edges and vertices of *G* are represented by *E* and *V*, respectively. *G* can be graphically depicted by circles representing *V* connected by line segments representing *E*. The adjacency matrix *M* of *G* is a square matrix of the size $|V|$ with elements e_{ij}. Since *G* is undirected, *M* is symmetrical around the main diagonal. Among *V*, we may distinguish minority and majority subsets such that $|V_{minority}| \ll |V_{majority}|$ and $|V_{minority}| + |V_{majority}| = |V|$. The edges amongst

members of these subsets form subgraphs within G are henceforth called *minority* and *majority partitions*. A third subgraph comprises of all of V but only edges between minority and majority nodes. Such a subgraph is called *interpartition*.

Dynamics on the graph

To each $v_i \in V$, an activation value is assigned according to Equation 2. The corresponding parameters values, i.e., coupling strength $\mathcal{E}$ and turbulence α, remain fixed in our model simulations. Models with identical parameter sets are called *families*. Five families of models are simulated, each with ten model instantiations, comprising a total of 50 model instantiations. Each network is run for 20 million iterations. All the simulations and analyses are conducted in R programming language version 3.6.0 (R Core Team, 2019) using computational resources provided by VSC (Flemish Supercomputer Center).

Parameter setting and Initialization

In our models, all *G* have $|\mathrm{V}| = 300$ and $|\mathrm{E}| = 5200$, a connectivity density providing robust evolution of small-world structure with uniform parameter setting (van den Berg et al., 2012). Model structure is initialized by randomly assigning $5200 \times 2 = 10400$ values "1" symmetrically to non-diagonal entries of *M*, and zeros to the remaining entries. Each node in the network is randomly assigned an initial value, uniformly distributed between 0 and 1, i.e., $x_{i_1} \underset{\sim}{iid}\ Unif(0,1)$.

Previous adaptive rewiring studies have been using values of α and $\mathcal{E}$ in the ranges of [1.7-1.9] and [0.3-05], respectively (Gong & van Leeuwen, 2003; Hellrigel et al., 2019; van den Berg & van Leeuwen, 2004). Here the midpoints of these ranges, i.e. α = 1.8 and $\mathcal{E}$ = 0.4, are used for the parameters in the baseline (BL) condition. In the BL condition, all nodes have the same parameter values.

The same applies to the majority (250 nodes) of the other conditions. However, depending on the condition, the minority subset (i.e., the first 50) of nodes could have either

lowered or increased values of either the α or $\mathcal{E}$ parameters. As shown in Figure S2, higher values of the turbulence parameter α tend to yield greater divergence; reducing the coupling parameter $\mathcal{E}$ has a similar effect (Hellrigel et al., 2019). Conditions with lowered values of α are called under-turbulent (UT), and those with increased values over-turbulent (OT); conditions with lowered $\mathcal{E}$ values are called under-coupled (UC) and those with increased values over-coupled (OC). While keeping the parameters of the majority at the baseline level ($\alpha_{i\in 51:300} = 1.8,\ \varepsilon_{i\in 51:300} = 0.4$) five different combinations of parameters were assigned to the minorities, each combination called a "family": The baseline family (BL; $\alpha_{i\in 1:50} = 1.8,\ \varepsilon_{i\in 1:50} = 0.4$), and the families with under-turbulent minority (UT; $\boldsymbol{\alpha_{i\in 1:50} = 1.7}$, $\varepsilon_{i\in 1:50} = 0.4$), over-turbulent family (OT; $\boldsymbol{\alpha_{i\in 1:50} = 1.9}$, $\varepsilon_{i\in 1:50} = 0.4$), under-coupled minorities (UC; $\alpha_{i\in 1:50} = 1.8,\ \boldsymbol{\varepsilon_{i\in 1:50} = 0.3}$), and over-coupled minority (OC; $\alpha_{i\in 1:50} = 1.8,\ \boldsymbol{\varepsilon_{i\in 1:50} = 0.5}$). In the Results section, we identify model instantiations by the two capitals indicating their family, together with a serial number [1-10], e.g. BL7, OT10. The 10 model instantiations within each condition are run with different initializations, which are identical across conditions to allow matched comparison between families.

Adaptive rewiring algorithm

A rewiring attempt takes place after every 20 updates of the logistic maps, meaning that over the 20 million updates of the model, one million rewiring attempts are performed. At each rewiring attempt, at time *t*, a node *i* is selected randomly from V, a vector of its distance from other nodes is calculated as $d_i = \left|X_t - x_{i,t}\right|$, and another vector of similarities is defined as $s_i = 1 - d_i$.

The most dissimilar neighbor and the most similar non-neighbor of node *i*, respectively denoted as δ and σ, are marked by finding the index of the maxima of the following vectors:

$$\delta = argmax(Md_i)$$

$$\sigma = argmax((1 - M)s_i)$$

The matrix multiplication of M and (1-M) with d_i and s_i, respectively, ensures that the search for the edges subject to rewiring happens in the right subset of edges. The rewiring is then changing the corresponding elements of the adjacency matrix:

$$M_{i\delta} = M_{\delta i} = 0$$

$$M_{i\sigma} = M_{\sigma i} = 1$$

Characterizing and comparing models

The state of each model at any given time *t* is described by adjacency matrix (M_t) (henceforth, "anatomical connectivity") which is subject to adaptive rewiring, and the vector of activation values, (X_t). Model's "functional connectivity" at *t*, (with adjacency matrix F_t) is defined by the momentary pairwise absolute differences of node activation values.

Qualitative description of network structures.

Network structure can be qualitatively assessed by means of visual inspection of the graph diagram or the adjacency matrix. Using the package *seriation* (Hahsler et al., 2008), the adjacency matrix is serialized by ordering rows and columns according to the projection of the matrix on its first principal component. Seriation maximizes visual identifiability of modules within the network.

Quantitative measures of the structure.

In network science, a wide range of structural measures of connectivity, also known as network statistics, have been proposed (Costa et al., 2007). After each rewiring attempt, we calculate six network connectivity measures: clustering coefficient, average path length, small-worldness, modularity, assortativity, and edge density Furthermore, we calculate an additional measure, namely, rich club coefficient, after the last rewiring attempt. All measures are calculated separately for the whole and the three subgraphs (viz., minority and

majority partition and the interpartition). Unless mentioned otherwise, the *igraph* package (Csardi & Nepusz, 2006) is used for calculating the measures.

Clustering coefficient.

This measure can be defined either locally or globally and gives an indication for the tendency of nodes to form clusters. We use the global clustering coefficient, which is defined as the number of closed triplets of nodes (the triplets of nodes that are all connected) divided by the number of connected triplets, either open (i.e., paths of length two) or closed (i.e., triangles). The numerator is equal to three times the number of triangles in the graph. Using linear algebra, the global clustering coefficient can be calculated formally from the adjacency matrix *M* as shown in Equation 3.

$$C = \frac{3 \times \#\, triangles}{\#\, triplets\ of\ connected\ nodes} = \frac{Tr(M^3)}{\Sigma M^2 - Tr(M^2)} \quad (3)$$

Trace of matrix A is defined as sum of diagonal elements of A, i.e., $Tr(A) = \sum_i A_{ii}$.

Average path length.

Average path length is the mean value of lengths of shortest path between all pairs of nodes, as defined in Equation 4 for a network of size *N*, where d_{ij} is the length of shortest distance between nodes *i* and *j*, and $d_{ij} = 0$ if there is no path between *i* and *j*. This measure gives an indication of how closely the nodes of a network are located from each other.

$$PL = \frac{1}{N(N-1)} \sum_{i \neq j \in V} d_{ij} \quad (4)$$

Small-worldness.

Small-worldness is a measure of the degree to which the graph shows properties akin to the structures known as *small world* (Watts & Strogatz, 1998). It is defined as the multiplication of normalized clustering coefficient and efficiency of the network as shown in Equation 5.

$$\mathrm{SW}_{norm} = \frac{C \times E}{C_0 \times E_0} \quad (5)$$

Efficiency of a network, *E*, quantifies the information exchange within the network and is defined as sum of inverses of the distances between nodes, normalized by network size, as shown in Equation 6 for a network with *N* nodes.

$$E = \frac{1}{N(N-1)} \sum_{i \neq j \in V} \frac{1}{d_{ij}} \quad (6)$$

d_{ij} is defined similar to Equation 4. C_0 and E_0 in the denominator of SW_{norm} are the expected clustering coefficient and efficiency of a random graph of the same as the graph in question. Since all networks modeled in this study start off with random networks of the same size and density, for computational reasons, a non-normalized version of small-worldness coefficient (i.e., $\mathrm{SW} = C \times E$) is calculated and reported.

Modularity.

Modularity of a graph, as proposed by Newman (2006) and denoted by *Q*, is a measure of to what extent the nodes tend to form interconnected communities isolated from the other nodes of the graph. More precisely, for a network of size *N* (with the theoretical maximum number of edges $m = \frac{N(N-1)}{2}$) and adjacency matrix *M*, modularity is defined as shown in Equation 7:

$$Q = \frac{1}{2m} \sum_{i,j} \left[M_{ij} - \frac{k_i k_j}{2m} \right] \delta(c_i, c_j) \quad (7)$$

In this equation, k_i and k_j are degrees of nodes *i* and *j*. $\delta(c_i, c_j)$ is the Kronecker delta function, which is equal to one if nodes *i* and *j* have the same label and zero otherwise. The term in the brackets is the difference between the actual number of edges between nodes *i* and *j* and the expected number of edges between them. Hence, according to Equation 7, modularity equals to the sum of these differences for the nodes within communities, normalized by the theoretical maximum number of edges in the network.

This measure requires a priori labeling of nodes that defines the communities to which the nodes are believed to belong. A variety of algorithms have been suggested to discover module, or communities, within a network so that the value of *Q* is maximized (for a review, cf. Zhang et al., 2018). The communities discovered by these algorithms can thus be used as labels for calculating modularity of the network. In line with Clauset et al. (2004), we use the fast greedy algorithm to optimally detect communities and thus calculate the modularity based on community membership of the nodes.

Assortativity.

Assortativity coefficient is a measure of homophily in networks that indicates the preferences of nodes to connect to "similar" nodes. The similarity can be imposed externally, e.g., by assigning categories to the nodes using labels (known as nominal assortativity), or by internal criteria such as node degrees (degree assortativity). Degree assortativity is defined as the Pearson correlation coefficient of degrees of connected nodes, thus taking values in the range <-1,1>.

To define it formally, let p_k be the probability that a randomly chosen node has degree k. It can be shown that the degree distribution for a node connected to a randomly selected edge *l* is thus proportional to kp_k. Then, a quantity for "remaining degree" is defined as $q_k = \frac{(k+1)p_{k+1}}{\sum_j jp_j}$ which is the normalized distribution of remaining degree for the nodes connected to *l*. Finally, the joint probability of remaining degrees of the nodes at both ends of *l* is denoted by e_{jk}. For an undirected network $e_{jk} = e_{kj}$ and its marginal distribution is $\sum_j e_{jk} = q_k$. Having the variance of remaining degree as $\sigma_q^2 = \sum_k k^2 q_k - [\sum_k k q_k]^2$, the degree assortativity can be calculated as shown in Equation 8 (Newman, 2003).

$$r = \frac{1}{\sigma_q^2} \sum_{ij} jk\left(e_{jk} - q_j q_k\right) \tag{8}$$

Edge density.

For a subset of nodes, this coefficient is the proportion of existing edges in a subgraph to the theoretical maximum number of edges possible in the same subgraph. For a subgraph with a subset of nodes $|V_s|$ and adjacency matrix M_s, this value is calculated as follows:

$$ED = \frac{\sum_{ij} M_s}{|V_s|(|V_s| - 1)} \tag{9}$$

Since the total number of edges remains the same during the adaptive rewiring, this coefficient gives an indication of how strongly each partition has attracted new nodes at every rewiring step.

Rich Club coefficient.

This coefficient quantifies the tendency of nodes with higher than a certain degree to connect to each other. More formally, as Equation 10 shows, it is equivalent to the edge density of the subgraph of the network where the nodes with lower degrees than the cut-off value *k* are removed. Since this coefficient is a function of club size *k*, it is hard to visualize its evolution over time for all possible values of *k*. Hence, the values of this coefficient were only plotted for the final state of the networks. We use the *brainGraph* package (Watson, 2019) to calculate rich club coefficient.

$$RC(k) = \frac{ED_{>k}}{\frac{N_{>k}(N_{>k} - 1)}{2}} \tag{10}$$

The absolute value of the rich club coefficient is hard to interpret and is not comparable among networks of different sizes, densities, and degree distributions. Hence, this coefficient is often normalized by the average rich club coefficient of random networks of the same size with similar degree sequence. We simulate 200 such networks for each model and, for each club size *k*, normalized the values of the rich club coefficients of the model by the average among the random networks. Moreover, for each *k*, we performed 1-

sample t-test to determine if the non-normalized *RC* is significantly higher than its average among the randomly generated networks.

For a certain k, a normalized rich club coefficient larger than one indicates that nodes with degree *k* tend to connect to the "rich" nodes (i.e., those with degrees equal to or higher than k), thus forming "rich clubs." Conversely, $RC_{norm}(k) < 1$ implies that the nodes with degree *k* show a tendency to connect to nodes with lower degrees. Finally, $RC_{norm}(k) = 1$ suggests that nodes with degree *k* show no preference to connect to nodes with lower or higher degrees.

Investigating resemblance between models

To studying the effect of heterogeneous parameterization of the models on their structures, we need to compare families with each other. In line with Berlingerio and colleagues (2012), we assume that the structural information embedded in networks can be summarized by the distributions of local network measures. Comparison of networks is thus reduced to comparing these distributions. To obtain measures of distributional distances, we use NetSimile (Berlingerio et al., 2012) and HHG (Heller et al., 2013) methods, detailed in the Supplementary Materials. NetSimile suggests the degree of dissimilarity between the distributions attributed to the networks being compared. HHG, on the other hand, provides p-values for a test of independence among the distributions; lower p-value derived from HHG (e.g., below the threshold of $\alpha = 0.05$) provides evidence in favor of distributional dependence. Thus, loosely speaking, HHG can be regarded as an indicator for dissimilarity; higher values of this measures entail smaller "resemblance" (or dependence) between the networks. Yet, interpreting HHG p-values as such measure is rather unorthodox and is hardly meaningful unless put in parallel with another dissimilarity measure such as NetSimile.

We first make pairwise comparisons among the 1225 unique pairs of model instantiations at their final state after 1 million rewiring attempts. Having quantitative

measures for dissimilarities among the networks, we quantify the within-family resemblances and between-family contrasts among the models. Finally, we define a score for family distinction in order to compare how families vary with respect to this measure.

Family resemblances and differentiations

The outcomes of pairwise comparison of the networks using NetSimile and HHG were stored in four 50×50 matrices of form $Dissimilarity_m^N$ for networks *N* (either *M* or *F*, respectively for anatomical and functional connectivities) based on method *m* (either NetSimile or HHG). To ease the visual comparison of these measures, the matrices of NetSimile distances, i.e., $Dissimilarity_{NetSimile}^M$ and $Dissimilarity_{NetSimile}^F$, were normalized by the highest value in each matrix so their values range from zero to one. Then, within- and between-family contrast aggregate scores were calculated by averaging the elements of dissimilarity matrices that belong to the families being compared as shown in Equation 11.

$$Contrast_m^N(f_i, f_j) = \frac{1}{10 \times 10} \sum_{i \epsilon f_i} \sum_{j \epsilon f_j} Dissimilarity_{m_{ij}}^N \tag{11}$$

Finally, a differentiation score was calculated for each family to quantify the degree to which models belonging to family f_i resemble each other and, at the same time, diverge from the members of other families, as shown in Equation 12.

$$Differentiation^N(f_i) = \frac{1 - Contrast_{NetSimile}^N(f_i, f_i)}{\frac{1}{4}\sum_{i \neq j}\left[1 - Contrast_{NetSimile}^N(f_i, f_j)\right]} \tag{12}$$

In this equation, the numerator is the within-family resemblance of networks belonging to family f_i. The denominator is the mean of between-family resemblance of f_i to other families. This score will be larger than one if family f_i differentiates from other families. For the lack of straightforward interpretation, this score was not calculated for HHG outcomes.

Results

Network structures

Using the *seriation* and *igraph* packages, we plot the raw (unserialized) and ordered (serialized) adjacency matrices and the graph diagrams of the anatomical connectivities at their final state. In the plots, the minority and majority nodes are colored sky blue and pink, respectively. In both matrix visualizations and graph diagrams, the within-minority and within-majority edges are colored blue and red, respectively. The inter-partition edges, connecting nodes of minority subset to nodes of majority, are colored green. Although there are variations among models, either within- or between-families, in all models (except for the OT2, OT3, UC1, and UC3; see below), several densely coupled sets of nodes, i.e., modules, emerged. These modules can be identified as squares in the serialized adjacency matrices. All plots are available online on the Open Science Framework (https://osf.io/625d8/). Figure 1 shows two representative networks per family. As evident in the plots, the networks manifest a range of different structures. Yet, similarities can be observed among models belonging to same families.

The baseline models (BL2 and BL8, Figure 1) typically include three densely coupled modules, and a few larger, sparser sets of nodes. The modules are not isolated from the rest of the network, as inter-modular edges keep them connected to other nodes. The unserialized adjacency matrices show that the density of edges are quite uniform over subsets of nodes.

In the OC family, wherein the minority nodes have relatively higher coupling strengths, the edge density is higher in the minority subgraph. Moreover, the OC family networks have more distinct modules than other families. OC2 (Figure 1), for instance, only has two modules, both of which are highly connected. Higher edge density in the minority subset and highly distinct modules are also the case for the UT family, which has lower turbulence parameter in the minority nodes (UT5 and UT 8, Figure 1). The similarity between

the OC and UT models was expected, as the nodes with lower turbulences and higher coupling strengths can synchronize more easily. However, it is interesting to note that the effect of better synchrony is not limited to the minority nodes; highly connected modules also emerge among the majority nodes.

In the OT family, the edge density is lower in the minority partition. Moreover, the higher level of turbulence parameter for minority nodes resulted in highly connected modules among the majority nodes (see OT4 in Figure 1). In the UC family, the edge density of the minority (which had lower coupling strengths) is lower than that of the majority. Moreover, lower coupling strength of the minority prevented minority nodes to form modules, and they were absorbed into modules formed mainly by the majority nodes. See UC5 and UC7 in Figure 1.

Network statistics

The evolution of clustering coefficient, modularity, edge density, small-world index, assortativity, and average path length were plotted for anatomical networks of all models and their sub-networks (viz., within-minority, within-majority, and interpartition). Figure 2 shows these plots for the minority, majority, and whole networks, stacked per family. The individual plots (including those of the interpartition sub-network) are available on the OSF repository. Furthermore, the normalized rich club coefficient of the final state of anatomical networks are plotted in Figure 3.

Let us first consider the evolution of network statistics for the whole networks. As evident in the plots, modularity, clustering coefficients, and small-worldness of all models increase noticeably after 60 thousand rewiring attempts (roughly by a factor of 4.7, 5.3, and 4.9, respectively) and degree assortativity approaches 0.53. Meanwhile, the average path length increases no more than 15%. The network statistics fluctuate afterward, and the fluctuation is more pronounced for degree assortativity. The majority subnetworks show

similar trends. In the minority subnetworks—although with higher fluctuations and instability in OC, UT, and UC—we observe an increase in these statistics after 60 thousand rewiring attempts. The network statistics of minority subnetworks of OT and BL families resemble those of the whole networks in the same families. Yet, clustering coefficient and small-worldness show higher growth in the minority subnetworks (more than 6- and 7-fold, respectively) and modularity is only moderately (roughly 35%) improved. The edge densities in the minority subnetworks, although unstable, are often large, roughly 2.4 times that of the whole network. In line with elevated edge density, average path length within the minority subgraph drops by almost 7%. This means that the minority nodes tend to connect more strongly to each other than to other nodes. Tables 1-3 summarize the mean and standard deviation of changes in network statistics after 60 thousand rewiring attempts for the whole network and the majority and minority subnetworks.

Figure 3 shows the normalized rich club coefficient $RC_{norm}(k)$ of the anatomical networks, grouped by families, as a function of club size *k*. $RC_{norm}(k)$ above one (dashed line) suggest existence of rich clubs. The values significantly larger than one ($p < 0.05$, based on 1-sample t-test) are marked by solid circles. Despite differences among families, they all show significant rich club structures for larger club sizes. More specifically, OC has clubs of sizes $80 < k < 145$, most of them significant, with consistent RC_{norm} values among members. Almost half of the UT models form rich clubs with $75 < k < 150$ yet others fail to. Other families, i.e., OT, BL, and UC, form clubs with of sizes ranging from 70 to roughly 135, with higher (but less consistent) RC_{norm} values compared to OC and UT. Fewer of $RC_{norm}(k > 70)$ are significant in OT, BL, and UC compared to OC.

Incidental losses

As can be observed in the evolution plots, four models (viz., OT2, OT3, UC1, and UC3) stop evolving before 10 thousand rewiring attempts. Visual inspection of their

anatomical connectivity reveals that, at some point in their evolution, one node reaches maximum degree and is connected to all other nodes (cf. Figure 4). Consequently, in the next rewiring step, the activation of an element of the coupled logistic map reaches singularity because of a zero by zero division which is mathematically undefined. The matrix operation in Equation 2 thus results in undefined values for activation of all other nodes at the next update of the logistic maps. These models fail to form any modules and were omitted from family-wise comparisons.

Family comparisons

NetSimile and HHG similarity measures were composed in new matrices wherein the lower triangle belongs to $Dissimilarity^N_{HHG}$ and the upper triangle belongs to $Dissimilarity^N_{NetSimile}$, i.e., $Dissimilarities^N = lower.tri(Dissimilarity^N_{HHG}) + upper.tri(Dissimilarity^N_{NetSimile})$. The matrices of $Dissimilarities^N$ are plotted in Figure 5 as heat maps using the *ComplexHeatmap* R package (Gu et al., 2016).

The matrices of $Contrast^N$ are plotted as upper triangular matrices in Figure 6. The cell colors, coded similarly to the heat maps, denote average contrast measures derived from NetSimile algorithm while average HHG p-values (i.e., $Contrast^N_{HHG}$) are indicated in each cell. The OC family manifests the least within-family contrast in the anatomical network. Based on the HHG test of multivariate independence, except for OC-OC and OC-UT family pairs in anatomical connectivities, no conclusive evidence exists for distributional dependence among families. Finally, as can be seen in this figure, the within- and between-family NetSimile contrasts of both anatomical and functional networks show similar patterns. More specifically, in both anatomical and functional networks, OC-BL, OC-UT, BL-BL, BL-UT, and UT-UT, all share close contrast values compared to other family pairs. This is also the case for BL-UC and UT-UC pairs.

The differentiation scores for both anatomical and functional connectivities of families are plotted in Figure 7. Differentiation values above one (dashed line) imply that the within-family resemblance of network structures of family f_i is higher than the average resemblance of its members to the members of other families. We observe elevated differentiations in both anatomical and functional networks of OC, BL, and UT. This measure is remarkably higher for the anatomical networks of the OC family while barely exceeding the threshold for the functional network of the same family.

Finally, in order to have both family resemblance and family differentiation in a single frame, we summarized their values in the graphs shown in Figure 8. In these graphs, individual nodes represent families of models. Edge color and size code between-family contrast and node color capture within-family contrast. The size of each node is proportional to the value of the differentiation score of its corresponding family. The families with $Differentiation^N(f_i) > 1$ are marked with asterisks. It can be noticed that in both anatomical and functional networks, the families with differentiation scores larger than one (i.e., OC, BL, and UT) have lower within-family contrast values. Moreover, the pairwise contrasts among these families (i.e., OC-BL, OC-UT, and BL-UT) are lower than any other family pair. This suggests that models with increased turbulence and decreased coupling strengths lead to structures less resembling the baseline family.

Discussion

We investigated the effect of non-uniformity of activity and connection strength on the evolution of network structure under adaptive rewiring. The adaptive rewiring was driven by synchronization in coupled logistic maps. The turbulence and coupling parameters of coupled logistic maps govern their synchronization behavior. It has amply been shown repeatedly that networks evolve to brain-like structure when these parameters were fixed to

uniform values. We replicated this behavior for our baseline parameter setting. Additionally, we studied how non-uniform parametrization reflects in network structure and whether adaptive rewiring algorithm is robust to these perturbations. To this aim, a minority subset of network units had either the turbulence parameter reduced (UT) or increased (OT), or the connectivity reduced (UC) or increased (OC). In all these conditions, adaptive rewiring evolves random networks into small-world structures with well-clustered modules and rich clubs. This evolution yields remarkable increase, as much as 5-fold, in clustering coefficient, network modularity, and small-worldness at the cost of a small (i.e., less than 15%) increase in average path length. Moreover, the models form rich clubs as large as 25-50% of network size. The evolution taking place in our models were in accordance with previous adaptive rewiring studies. Adaptive rewiring, therefore, is robust against symmetry-breaking perturbations of system parameters

Despite this overall consistency, we observed considerable variability among models, both in their evolution and the final states of structural and functional connectivity. These variations are partly due to the family-specific parameterization of models and partly to the random initialization of the models. We quantified the within- and between-family contrasts, and defined a measure of family differentiation, in order to score, on average, how well models belonging to one family distinguish from others.

We found that the baseline family and families with increased coupling strengths or decreased turbulence parameter (respectively, BL, OC, and UT) differentiate themselves most from other families, both in anatomical and functional connectivities. The differentiation score is highest for the anatomical connectivity of the OC family. Moreover, we observe rather high resemblance between OC and UT for both anatomical and functional connectivities. Based on the HHG test, there is rather strong evidence ($p = 0.02$) for distributional dependence between anatomical networks of OC and UT. This means that

elevated coupling strength and reduced turbulence have similar effect on the structure and activations of logistic maps.

Altogether, perturbation to the parameters of coupled logistic maps yields structural and functional differences that are essential for implementing cognitive functions in evolving networks. Moreover, for both the structural and functional networks, perturbation leads to differentiation of the network structure from the baseline. Different perturbations yield distinct structures. From a cognitive neuroscience perspective, this implies that functional and structural differentiation can be used to identify functional components in a network, in accord with the use of structural and functional connectivity measures in neuroimaging. In combination with the robustness of the models, this can be seen as added evidence favoring the role of synchrony in plasticity.

Concluding Remarks

Further research may extend our findings in several ways. Firstly, the incidental occurrence of network evolution breakdown was unexpected. Technically speaking, the matrix algebraic implementation of coupled logistic maps is sensitive to small computational errors such as undefined division for one node, as was the case for OT2, OT3, UC1, and UC3. A different implementation could have prevented breakdown by isolating the problematic node and proceeding the adaptive rewiring algorithm with the remaining network. However, a more principled solution may be called for. This may require a systematic study of the probability distribution of network breakdown under a range of parametrization conditions, network sizes, and connectivity densities.

Secondly, a broader range of parameter variation conditions than currently imposed should be attempted. For instance, turbulence and coupling strength parameters could both deviate from baseline values simultaneously, either for the same subset of nodes or for two

(overlapping or nonoverlapping) subsets. Random and patterned deviations of parameters can be studied in large-scale systems to implement perceptual and memory functions. Ultimately, the aim is to have these functions implemented in a network that simultaneously maintains its optimal structure.

Finally, this study was limited to binary, unweighted networks. The effect of non-uniform parameters of logistic maps can be studied, via systematic search, on weighted networks with various edge weight distributions, akin to Hellrigel et al. (2019).

We followed the strategy to provide the simplest possible model of brain structure and function, in order to avoid stacking of arbitrary assumptions. Simplification is inevitable in modeling; “all models are wrong—but some are useful.” (Attributed to George Box.) For those who consider the model to pose serious limitations on generalization of our findings to neurobiological systems, more realistic neural mass models instead of coupled maps could be a viable solution, in particular, ones that have facilities for studying traveling waves and phase-amplitude-frequency coupling (Chehelcheraghi et al., 2016, 2017).

Data and Code Availability

The reproducible scripts used in this study are available online on GitHub (https://github.com/psyguy/KUL-MPsy-Thesis) and on the study’s repository on the Open Science Framework (https://osf.io/625d8/). This repository also includes all model files generated in this study and additional plots of various qualitative and quantitative network measures.

References

Avena-Koenigsberger, A., Misic, B., & Sporns, O. (2018). Communication dynamics in complex brain networks. *Nature Reviews Neuroscience*, *19*(1), 17.

Berlingerio, M., Koutra, D., Eliassi-Rad, T., & Faloutsos, C. (2012). NetSimile: A Scalable Approach to Size-Independent Network Similarity. *ArXiv:1209.2684 [Physics, Stat]*. http://arxiv.org/abs/1209.2684

Bi, G., & Poo, M. (2001). Synaptic Modification by Correlated Activity: Hebb's Postulate Revisited. *Annual Review of Neuroscience*, *24*(1), 139–166. https://doi.org/10.1146/annurev.neuro.24.1.139

Breakspear, M., Terry, J. R., & Friston, K. J. (2003). Modulation of excitatory synaptic coupling facilitates synchronization and complex dynamics in a biophysical model of neuronal dynamics. *Network: Computation in Neural Systems*, *14*(4), 703–732. https://doi.org/10.1088/0954-898X_14_4_305

Brill, B., Heller, Y., & Heller, R. (2018). Nonparametric Independence Tests and k-sample Tests for Large Sample Sizes Using Package HHG. *The R Journal*, *10*(1), 424. https://doi.org/10.32614/RJ-2018-008

Butz, M., Wörgötter, F., & van Ooyen, A. (2009). Activity-dependent structural plasticity. *Brain Research Reviews*, *60*(2), 287–305. https://doi.org/10.1016/j.brainresrev.2008.12.023

Chehelcheraghi, M., Leeuwen, C. van, Steur, E., & Nakatani, C. (2017). A neural mass model of cross frequency coupling. *PLOS ONE*, *12*(4), e0173776. https://doi.org/10.1371/journal.pone.0173776

Chehelcheraghi, M., Nakatani, C., Steur, E., & van Leeuwen, C. (2016). A neural mass model of phase–amplitude coupling. *Biological Cybernetics*, *110*(2), 171–192. https://doi.org/10.1007/s00422-016-0687-5

Clauset, A., Newman, M. E. J., & Moore, C. (2004). Finding community structure in very large networks. *Physical Review E*, *70*(6), 066111. https://doi.org/10.1103/PhysRevE.70.066111

Costa, L. da F., Rodrigues, F. A., Travieso, G., & Villas Boas, P. R. (2007). Characterization of complex networks: A survey of measurements. *Advances in Physics*, *56*(1), 167–242. https://doi.org/10.1080/00018730601170527

Csardi, G., & Nepusz, T. (2006). The igraph software package for complex network research. *InterJournal*, *Complex Systems*, 1695.

Gong, P., & van Leeuwen, C. (2003). Emergence of scale-free network with chaotic units. *Physica A: Statistical Mechanics and Its Applications*, *321*(3), 679–688. https://doi.org/10.1016/S0378-4371(02)01735-1

Gong, P., & van Leeuwen, C. (2004). Evolution to a small-world network with chaotic units. *EPL (Europhysics Letters)*, *67*(2), 328. https://doi.org/10.1209/epl/i2003-10287-7

Heller, R., Heller, Y., & Gorfine, M. (2013). A consistent multivariate test of association based on ranks of distances. *Biometrika*, *100*(2), 503–510. https://doi.org/10.1093/biomet/ass070

Hellrigel, S., Jarman, N., & van Leeuwen, C. (2019). Adaptive rewiring in weighted networks. *Cognitive Systems Research*, *55*, 205–218. https://doi.org/10.1016/j.cogsys.2019.02.004

Jarman, N., Steur, E., Trengove, C., Tyukin, I. Y., & van Leeuwen, C. (2017). Self-organisation of small-world networks by adaptive rewiring in response to graph diffusion. *Scientific Reports*, *7*(1), 13158. https://doi.org/10.1038/s41598-017-12589-9

Jarman, N., Trengove, C., Steur, E., Tyukin, I., & van Leeuwen, C. (2014). Spatially constrained adaptive rewiring in cortical networks creates spatially modular small

world architectures. *Cognitive Neurodynamics*, *8*(6), 479–497. https://doi.org/10.1007/s11571-014-9288-y

Jurman, G., Riccadonna, S., Visintainer, R., & Furlanello, C. (2009). Canberra distance on ranked lists. *Proceedings of Advances in Ranking NIPS 09 Workshop*, 22–27.

Kaneko, K. (1992). Overview of coupled map lattices. *Chaos: An Interdisciplinary Journal of Nonlinear Science*, *2*(3), 279–282. https://doi.org/10.1063/1.165869

Meunier, D., Lambiotte, R., & Bullmore, E. T. (2010). Modular and Hierarchically Modular Organization of Brain Networks. *Frontiers in Neuroscience*, *4*. https://doi.org/10.3389/fnins.2010.00200

Newman, M. E. J. (2003). Mixing patterns in networks. *Physical Review E*, *67*(2), 026126. https://doi.org/10.1103/PhysRevE.67.026126

Newman, M. E. J. (2006). Modularity and community structure in networks. *Proceedings of the National Academy of Sciences*, *103*(23), 8577–8582. https://doi.org/10.1073/pnas.0601602103

Papadopoulos, L., Kim, J. Z., Kurths, J., & Bassett, D. S. (2017). Development of structural correlations and synchronization from adaptive rewiring in networks of Kuramoto oscillators. *Chaos: An Interdisciplinary Journal of Nonlinear Science*, *27*(7), 073115. https://doi.org/10.1063/1.4994819

R Core Team. (2019). *R: A language and environment for statistical computing*. https://www.R-project.org/

Rubinov, M., Sporns, O., van Leeuwen, C., & Breakspear, M. (2009). Symbiotic relationship between brain structure and dynamics. *BMC Neuroscience*, *10*(1), 55. https://doi.org/10.1186/1471-2202-10-55

Sporns, O., & Zwi, J. D. (2004). The small world of the cerebral cortex. *Neuroinformatics*, *2*(2), 145–162. https://doi.org/10.1385/NI:2:2:145

van den Berg, D., Gong, P., Breakspear, M., & van Leeuwen, C. (2012). Fragmentation: Loss of global coherence or breakdown of modularity in functional brain architecture? *Frontiers in Systems Neuroscience*, *6*. https://doi.org/10.3389/fnsys.2012.00020

van den Berg, D., & van Leeuwen, C. (2004). Adaptive rewiring in chaotic networks renders small-world connectivity with consistent clusters. *EPL (Europhysics Letters)*, *65*(4), 459. https://doi.org/10.1209/epl/i2003-10116-1

van den Heuvel, M. P., & Sporns, O. (2011). Rich-Club Organization of the Human Connectome. *Journal of Neuroscience*, *31*(44), 15775–15786. https://doi.org/10.1523/JNEUROSCI.3539-11.2011

van Leeuwen, C., & Raffone, A. (2001). Coupled nonlinear maps as models of perceptual pattern and memory trace dynamics. *Cognitive Processing*, *2*, 67–116.

van Leeuwen, C., Steyvers, M., & Nooter, M. (1997). Stability and Intermittency in Large-Scale Coupled Oscillator Models for Perceptual Segmentation. *Journal of Mathematical Psychology*, *41*(4), 319–344. https://doi.org/10.1006/jmps.1997.1177

van Strien, S. J. (1987). *Smooth Dynamics on the Interval (with an Emphasis on Unimodal Maps)*. Delft University of Technology.

Watson, C. G. (2019). *brainGraph: Graph theory analysis of brain MRI data*. https://github.com/cwatson/brainGraph

Watts, D. J., & Strogatz, S. H. (1998). Collective dynamics of 'small-world' networks. *Nature*, *393*(6684), 440–442. https://doi.org/10.1038/30918

Zhang, X., Ma, Z., Zhang, Z., Sun, Q., & Yan, J. (2018). A Review of Community Detection Algorithms Based on Modularity Optimization. *Journal of Physics: Conference Series*, *1069*, 012123. https://doi.org/10.1088/1742-6596/1069/1/012123

Tables

Table 1

Means and standard deviations (between parentheses) of network statistics of the whole graph for different conditions.

Condition	Clustering	Average path length	Small-worldness	Modularity	Assortativity	Edge density
OC	5.33(1.05)	1.15(0.05)	4.86(0.88)	4.69(0.85)	0.52(0.22)	1(0.02)
OT	5.34(1.02)	1.15(0.05)	4.87(0.86)	4.7(0.81)	0.53(0.22)	1(0.01)
BL	5.32(1.05)	1.14(0.05)	4.85(0.88)	4.68(0.84)	0.53(0.22)	1(0.02)
UT	5.35(1.03)	1.15(0.05)	4.87(0.86)	4.7(0.82)	0.53(0.22)	1(0.02)
UC	5.35(1.01)	1.15(0.05)	4.88(0.85)	4.69(0.82)	0.53(0.22)	1(0.01)
OC	5.33(1.05)	1.15(0.05)	4.86(0.88)	4.69(0.85)	0.52(0.22)	1(0.02)

Note: Means are from 60 thousand to one million rewiring steps, normalized by those of 100 random networks, except degree assortativity. BL: baseline; UT: under-turbulent; OT: over-turbulent; UC: under-coupled; OC: over-coupled.

Table 2

Means and standard deviations (between parentheses) of network statistics of the majority subgraph for different conditions.

Condition	Clustering	Average path length	Small-worldness	Modularity	Assortativity	Edge density
OC	5.49(1.13)	1.17(0.06)	4.91(0.92)	4.45(0.84)	0.52(0.18)	1.01(0.12)
OT	5.51(1.08)	1.17(0.06)	4.93(0.89)	4.47(0.8)	0.52(0.18)	1(0.11)
BL	5.49(1.12)	1.17(0.06)	4.9(0.92)	4.44(0.83)	0.52(0.18)	1.01(0.12)
UT	5.52(1.11)	1.18(0.06)	4.93(0.91)	4.47(0.81)	0.53(0.18)	1(0.12)
UC	5.53(1.08)	1.18(0.06)	4.94(0.89)	4.46(0.8)	0.54(0.18)	1(0.12)
OC	5.49(1.13)	1.17(0.06)	4.91(0.92)	4.45(0.84)	0.52(0.18)	1.01(0.12)

Note: Means are from 60 thousand to one million rewiring steps, normalized by those of 100 random networks, except degree assortativity. BL: baseline; UT: under-turbulent; OT: over-turbulent; UC: under-coupled; OC: over-coupled .

Table 3

Means and standard deviations (between parentheses) of network statistics of the minority subgraph for different conditions.

Condition	Clustering	Average path length	Small-worldness	Modularity	Assortativity	Edge density
OC	6.24(1.71)	0.94(0.24)	7.45(3.19)	1.35(0.56)	0.53(0.32)	2.36(1.44)
OT	6.26(1.69)	0.93(0.24)	7.57(3.25)	1.35(0.57)	0.53(0.31)	2.42(1.49)
BL	6.18(1.72)	0.94(0.24)	7.42(3.14)	1.38(0.54)	0.52(0.32)	2.35(1.39)
UT	6.19(1.7)	0.93(0.23)	7.41(3.12)	1.39(0.52)	0.52(0.32)	2.34(1.38)
UC	6.2(1.67)	0.93(0.24)	7.44(3.2)	1.37(0.55)	0.51(0.31)	2.36(1.47)
OC	6.24(1.71)	0.94(0.24)	7.45(3.19)	1.35(0.56)	0.53(0.32)	2.36(1.44)

Note: Means are from 60 thousand to one million rewiring steps, normalized by those of 100 random networks, except degree assortativity. BL: baseline; UT: under-turbulent; OT: over-turbulent; UC: under-coupled; OC: over-coupled .

Figures

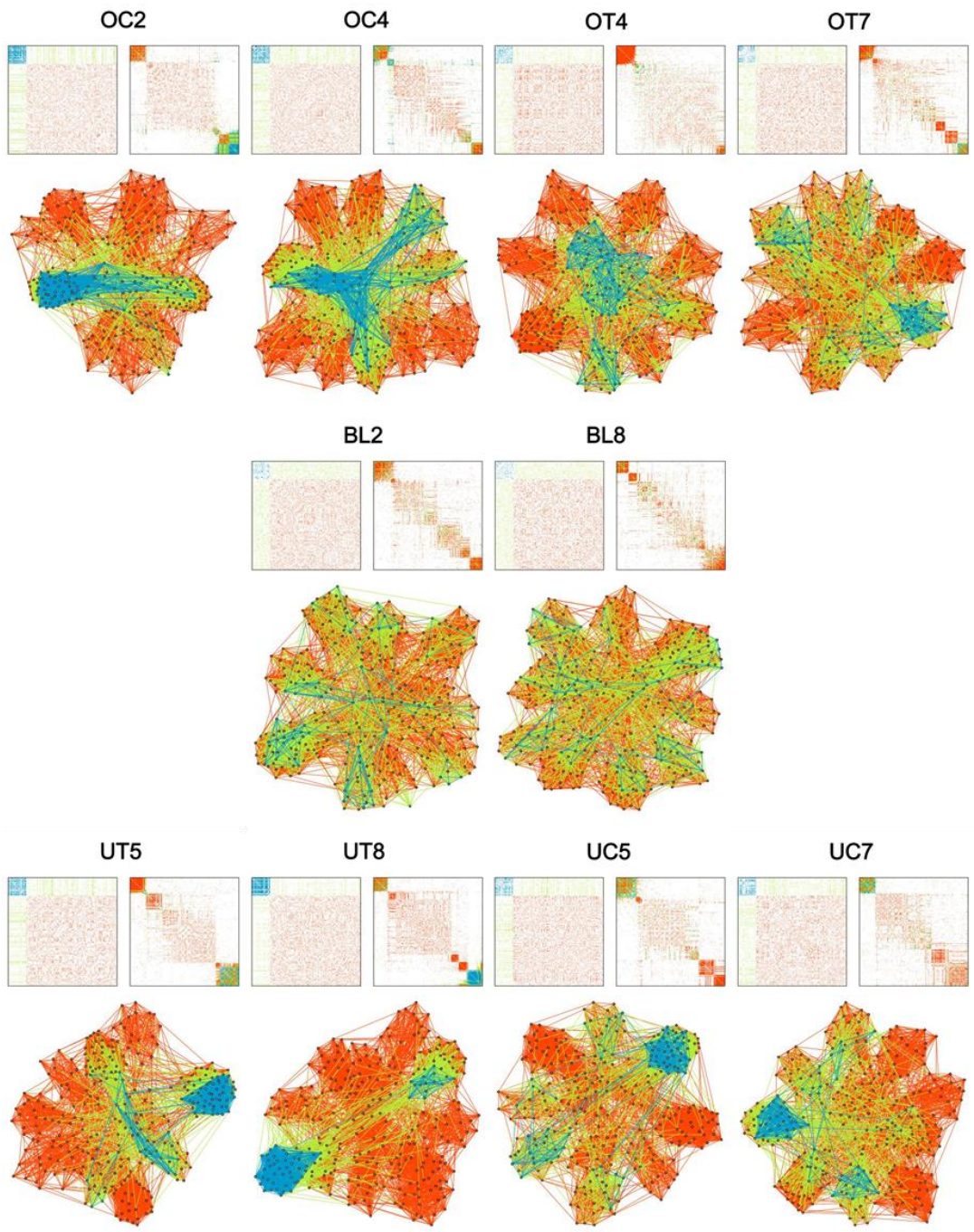

Figure 1. Network structures of representative models. Each panel shows the unserialized (top left) and serialized (top right) adjacency matrices, and the graph representation (bottom) of the structural connectivity at the last rewiring step. The within-minority, within-majority, and interpartition edges are colored blue, red, and green, respectively. In the graph representation, the minority and majority nodes are colored sky blue and pink, respectively.

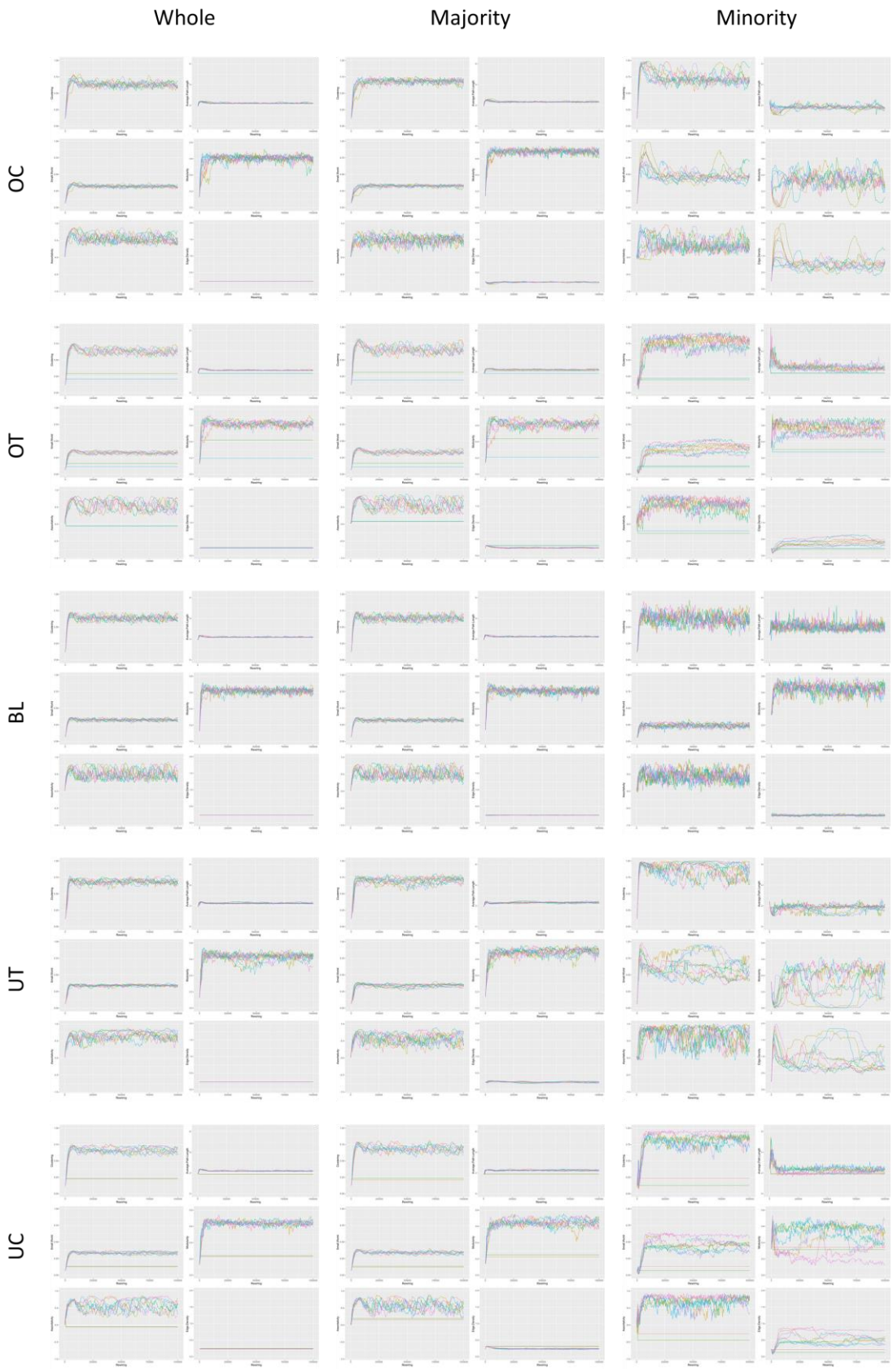

Figure 2. Evolution of network statistics for the whole network and majority and minority subgraphs, grouped by condition.

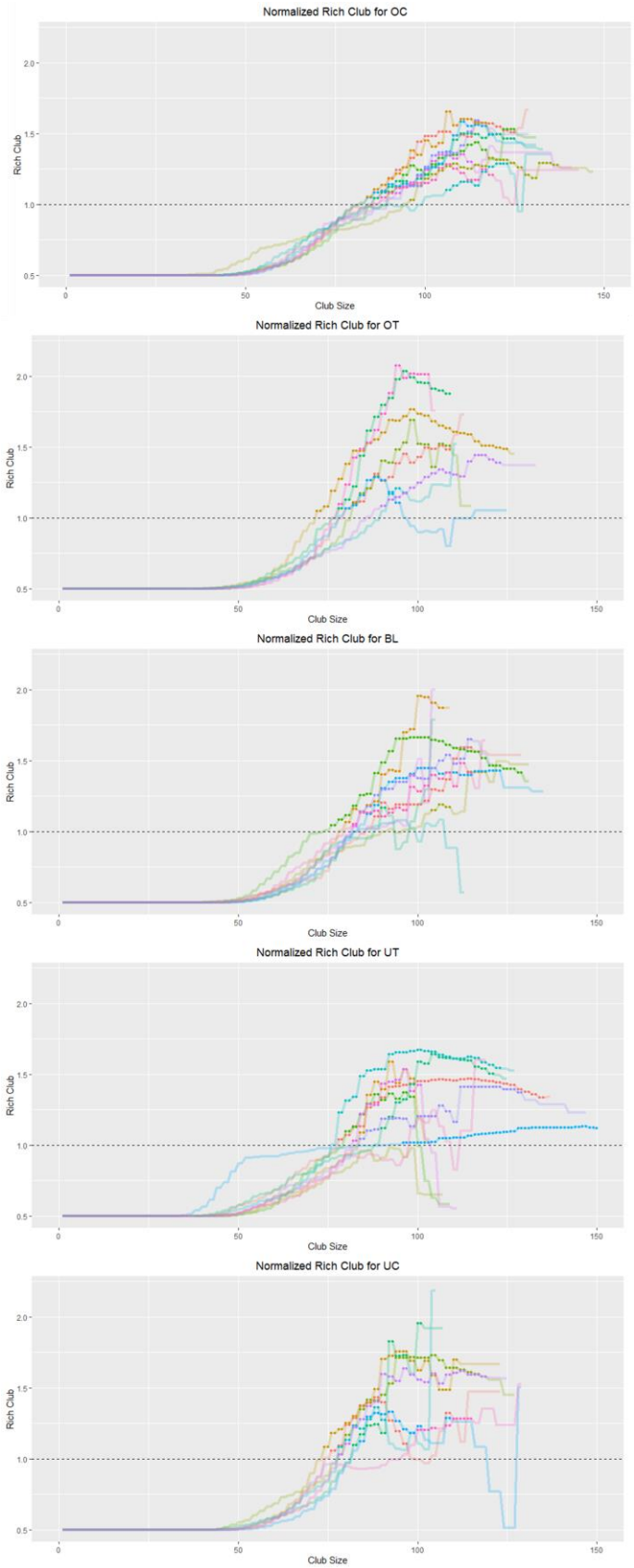

Figure 3. Normalized rich club coefficients of the whole network after the last rewiring step, grouped by condition. Significant values are marked by solid circles.

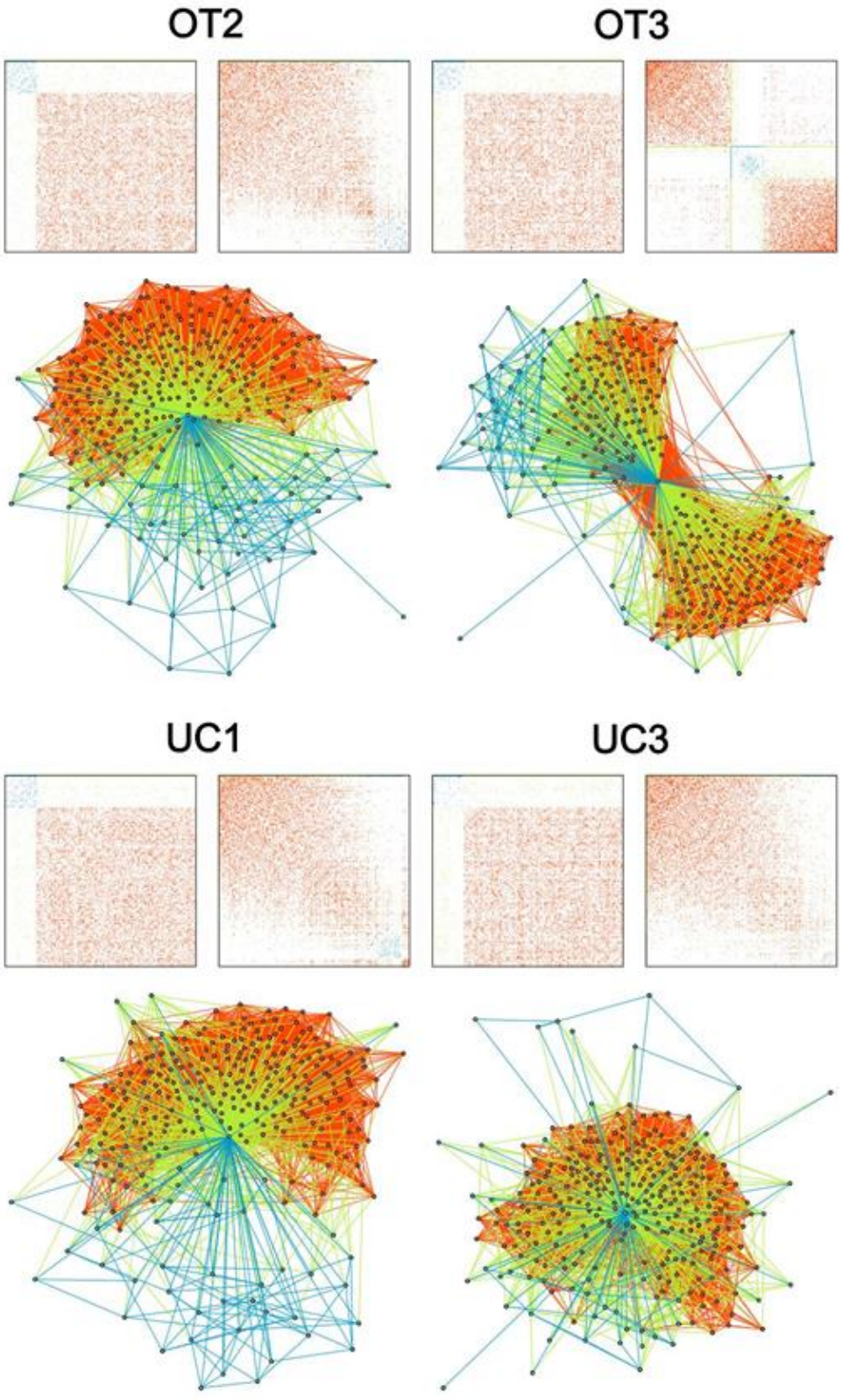

Figure 4. Network structures of terminated models. Panels and color coding are similar to those of Figure 2.

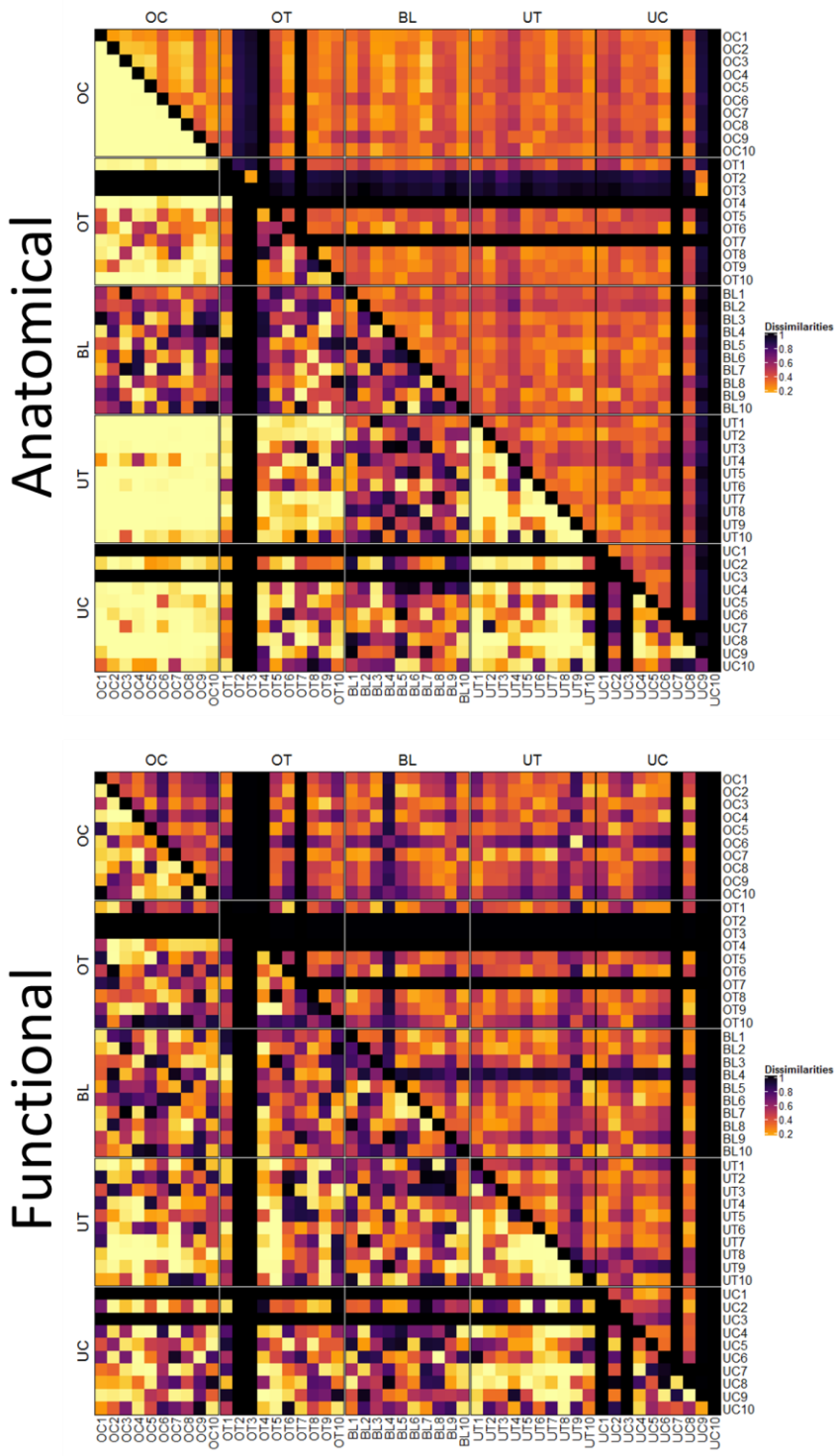

Figure 5. Heat maps of pairwise dissimilarities of anatomical (top) and functional (bottom) networks. The upper diagonal elements show normalized dissimilarity measures derived from NetSimile algorithm, and the lower diagonal elements show HHG p-values. Model names and family assignment are indicated. Lower dissimilarity (hence higher similarity) measures are coded by brighter colors.

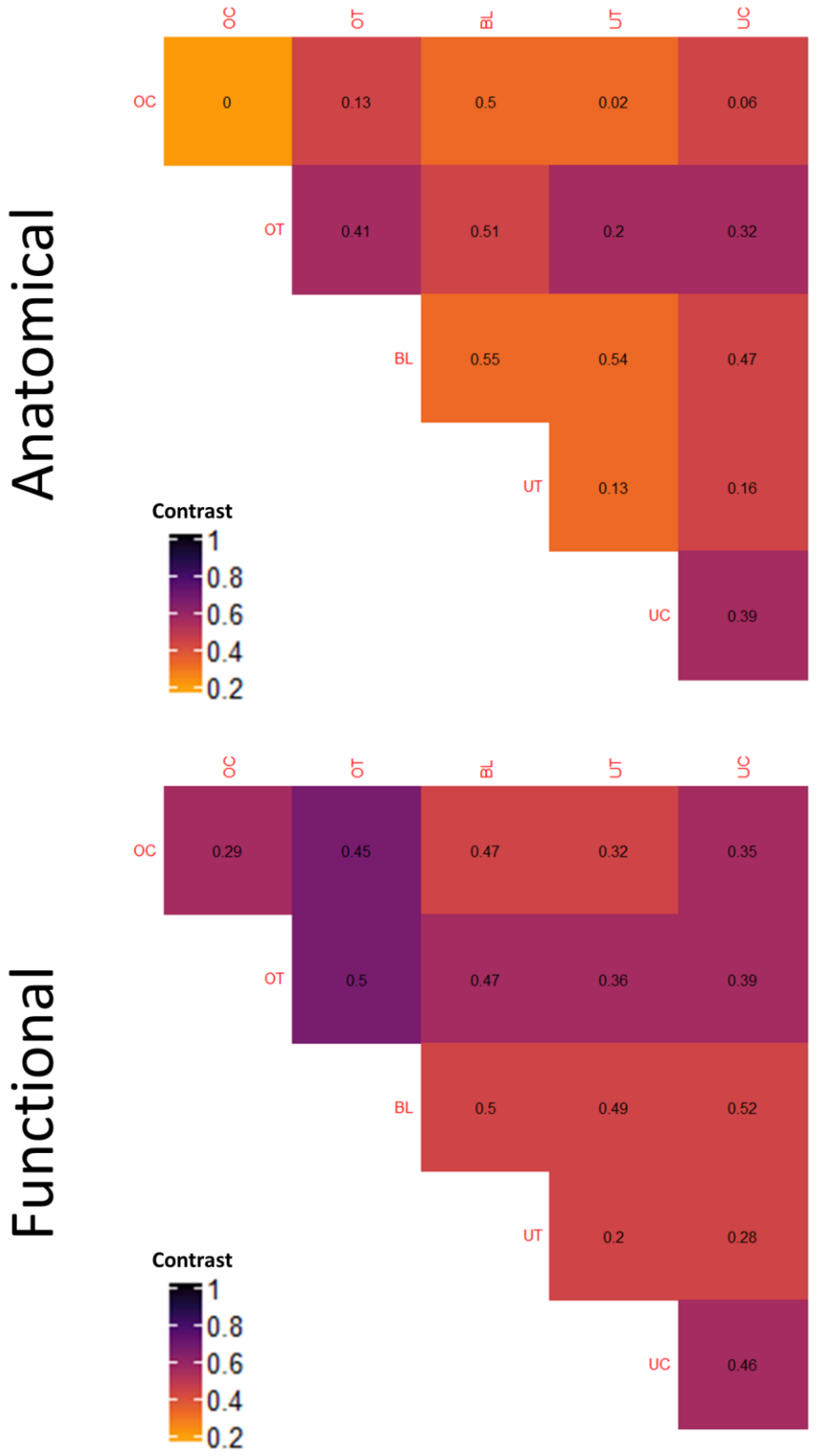

Figure 6. Heat maps of within- and between-family contrasts for anatomical (top) and functional (bottom) connectivities. The values within cells show the average HHG p-values of corresponding family-wise comparisons. Lower contrast measures are coded by brighter colors.

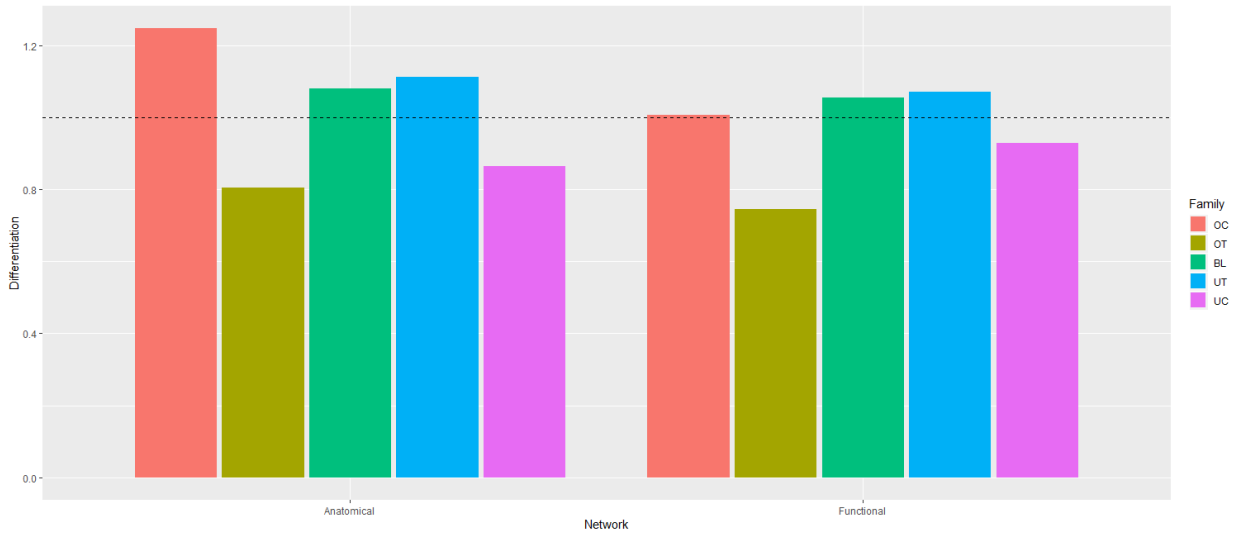

Figure 7. Between-families differentiation score of for anatomical and functional networks. Values above one (dashed line) imply above-average within-family resemblance compared to other families.

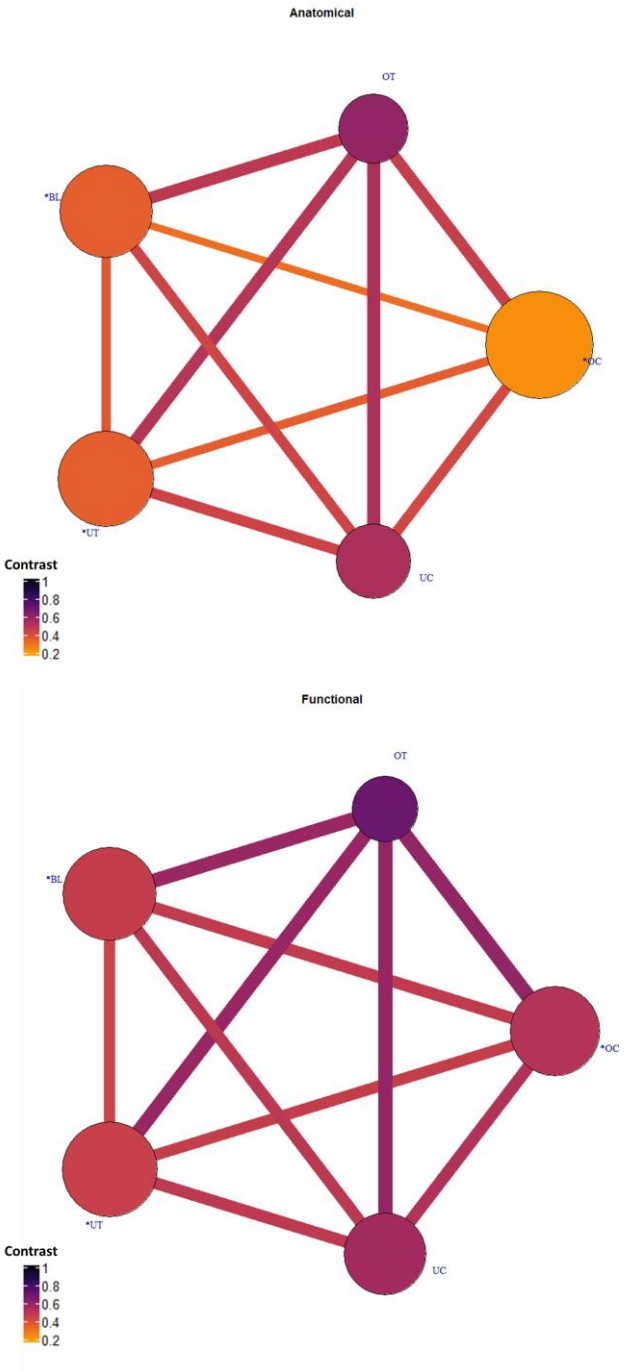

Figure 8. Graph representation of family resemblance and differentiation in anatomical (top) and functional (bottom) connectivities of fully evolved models. Edge color and size code between-family contrast and node color captures within-family contrast. Node size is proportional to the differentiation score of corresponding family. The families with differentiation scores above one are marked with asterisks.

Supplementary Materials

Methods

Networks as distributions.

Network statistics can describe network structures either locally or globally. Local measures are suitable for node-wise (or clique-wise) comparisons, while the global measures are aggregates of some local properties that provide "summary statistics" for the structure. Whereas local measures hardly lead to holistic description of networks (as the nodes are usually described in isolation from other nodes) in their aggregation for deriving global measures, structural information is sacrificed. Therefore, neither local nor global measures are optimally suitable for comparison of networks. A possible solution is to use the distribution of several local measures for network comparison.

Berlingerio et al. (2012) suggest characterizing each node *i* of the network with a seven-dimensional feature vector consisting of the following local measures that capture characteristics of the node and its surrounding subset of the network: $d_i = |N(i)|$[1], degree (i.e., number of neighbors); c_i, local clustering coefficient (i.e., the number of triangles connected to node *i* over the number of connected triples centered on node *i*); $\overline{d_{N(i)}} = \frac{1}{d_i}\sum_{\forall j \in N(i)} d_j$, average degree of node's neighbors; $\overline{c_{N(i)}} = \frac{1}{d_i}\sum_{\forall j \in N(i)} c_j$, average clustering coefficient of node's neighbors; $|E_{ego(i)}|$, the number of edges in the egonet[2] of node *i*; $|E^{\circ}{}_{ego(i)}|$, the number of outgoing edges from the egonet of node *i*; and $|N(ego(i))|$, the number of neighbors of egonet of node *i*. Although more local features could be added to this

[1] N(i) is the set of first-order neighbors of node *i*, i.e., the nodes directly connected to *i*.

[2] Egonet of node *i*, referred to as ego(i), is the subset of the network including node *i*, its first-order neighbors (N(i)), and the edges among N(i).

vector, Berlingerio and colleagues have shown that these features suffice in practice for comparison of networks.

The NetSimile method.

The distribution of local features enables the comparison of their summary statistics. In NetSimile (Berlingerio et al., 2012), the feature distribution (which is a $nodes \times features$ matrix) is aggregated into a 35-dimensional signature vector consisting of five summary statistics for each feature: median, mean, standard deviation, skewness, and kurtosis. The comparison of networks is thus reduced to calculating distances (or similarities) of the signature vectors. NetSimile is superior to other methods of inferring network similarity as its computational complexity grows linearly with the size of the networks, and more importantly, it allows comparison of networks of different sizes.

Ranks and values of summary statistics characterize the overall shape of distributions and thus are highly diagnostic for their comparison (Berlingerio et al., 2012). Hence, the signature vectors are akin to ranked lists. It has been shown that the Canberra distance, defined in Equation S1, is an appropriate measure of dissimilarity for ranked lists (Jurman et al., 2009) as it is sensitive to small distances from zero and normalizes the pairwise distances of features by their absolute values. Moreover, Berlingerio and colleagues (2012) report high discriminative power of Canberra distance in comparison of signature vectors, a good property of a dissimilarity measure for the task at hand.

$$Ca(\boldsymbol{x}, \boldsymbol{y}) = \sum_{i=1, |x_i|+|y_i| \neq 0}^{n} \frac{|x_i - y_i|}{|x_i| + |y_i|} \tag{S1}$$

We use this dissimilarity metric in the pairwise comparison of the signature vectors derived from NetSimile algorithm. However, NetSimile does not allow hypothesis testing to infer significance levels for the distances. Berlingerio et al. (2012) suggest hypothesis testing for independence of the distributions by pairwise comparison of the univariate distributions

of the features and aggregating their p-values through averaging or choosing the maximum values. They report that neither Mann-Whitney nor Kolmogorov-Smirnov tests—which are nonparametric tests without any assumption for the distributions being compared—yield amply meaningful discrimination among the networks being compared. Their approach of hypothesis testing ignores the multivariate dependencies of the features. Hence, we use another method to test independence of distributions that is discussed below.

Hypothesis testing for similarities of network distributions.

The significance tests used by Berlingerio et al. (2012) posits multivariate independence among features and lacks what they call "discrimination power." To tackle this issue, one needs use multivariate dependence tests. Since parametric dependence tests rely on assumption for the distributions being compared, we used HHG nonparametric permutation test of multivariate dependence (Heller et al., 2013) implemented in *HHG* R package (Brill et al., 2018). HHG is a consistent omnibus test for the null hypothesis of distributional independence, i.e., that the joint distribution of two multivariate random variables X and Y is equal to the multiplication of the marginal distributions of those variables. Equation S2 shows the null and alternative hypotheses:

$$\begin{cases} H_0: F_{XY}(x,y) = F_X(x)F_Y(y) \\ H_1: F_{XY}(x,y) \neq F_X(x)F_Y(y) \end{cases} \quad \forall x, y \tag{S2}$$

HHG has a reasonable computational complexity and uses norm distance matrices of the samples taken from X and Y separately. The technical details of this method are beyond the scope of this paper. In short, HHG iteratively forms hyper spheres in the joint space of $F_{XY}(x,y)$ and based on the implications of the null hypothesis, quantifies evidence against H_0 by likelihood ratio or Pearson's Chi-square tests statistics over contingency tables. From these tests, one can drive permutation p-values that can be interpreted as evidence against null hypothesis of the independence of the distributions. Hence, the lower the p-value, the more evidence favoring the dependence of the distributions being compared. Loosely

speaking, one can treat the p-values derived from HHG methods as a form of distributional dissimilarity; the lower the value, the more "similar" the distributions are to each other. This interpretation allows us to compare non-significant p-values as relative measures of resemblance.

The *hhg.test()* function in *HHG* package runs the test for a number of permutations on distance matrices of the samples in X and Y and outputs four different permutation p-values based on sums or maximum values of likelihood ratio or Chi-square test scores of all 2×2 contingency tables. We let HHG run for 2000 permutations for each pairwise comparison and extracted permutation p-value for the maximum of likelihood ratio score statistics as it yielded higher discriminative power compared to other test statistics.

Supplementary references

Berlingerio, M., Koutra, D., Eliassi-Rad, T., & Faloutsos, C. (2012). NetSimile: A Scalable Approach to Size-Independent Network Similarity. *ArXiv:1209.2684 [Physics, Stat]*. http://arxiv.org/abs/1209.2684

Breakspear, M., Terry, J. R., & Friston, K. J. (2003). Modulation of excitatory synaptic coupling facilitates synchronization and complex dynamics in a biophysical model of neuronal dynamics. *Network: Computation in Neural Systems*, *14*(4), 703–732. https://doi.org/10.1088/0954-898X_14_4_305

Brill, B., Heller, Y., & Heller, R. (2018). Nonparametric Independence Tests and k-sample Tests for Large Sample Sizes Using Package HHG. *The R Journal*, *10*(1), 424. https://doi.org/10.32614/RJ-2018-008

Heller, R., Heller, Y., & Gorfine, M. (2013). A consistent multivariate test of association based on ranks of distances. *Biometrika*, *100*(2), 503–510. https://doi.org/10.1093/biomet/ass070

Jurman, G., Riccadonna, S., Visintainer, R., & Furlanello, C. (2009). Canberra distance on ranked lists. *Proceedings of Advances in Ranking NIPS 09 Workshop*, 22–27.

Rubinov, M., Sporns, O., van Leeuwen, C., & Breakspear, M. (2009). Symbiotic relationship between brain structure and dynamics. *BMC Neuroscience*, *10*(1), 55. https://doi.org/10.1186/1471-2202-10-55

Supplementary figures

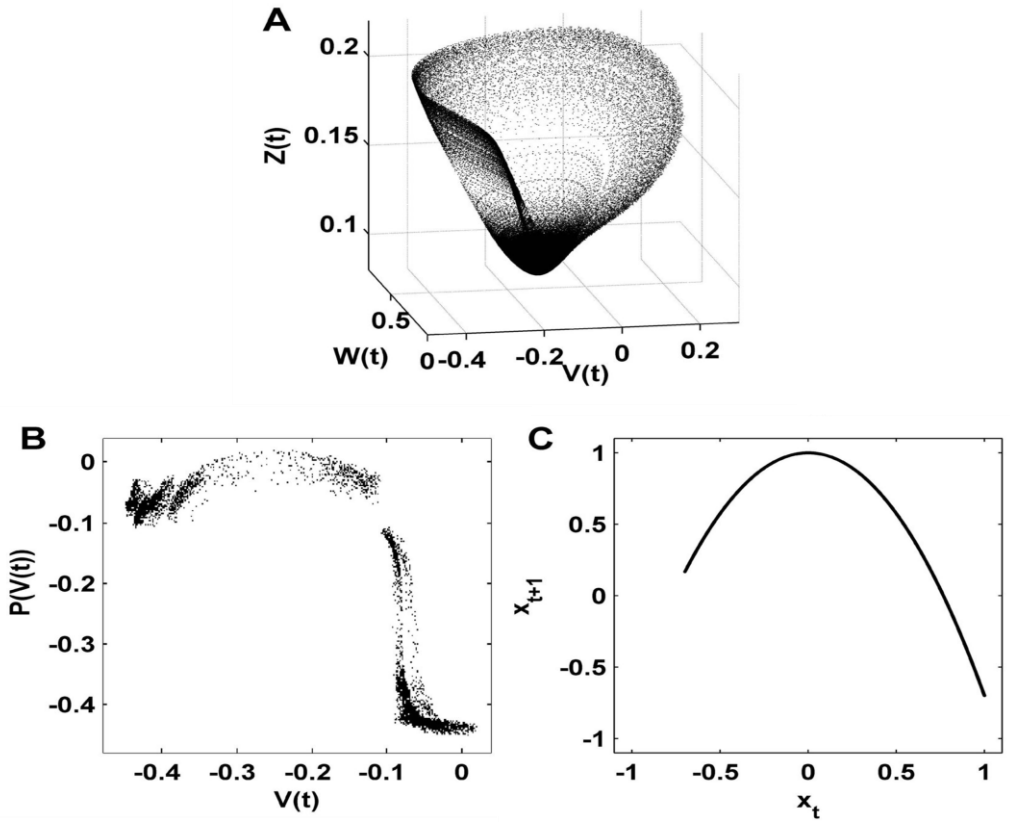

Figure S1. Dimension reduction of nonlinear neuronal dynamics. (A) Phase space attractor of a three-dimensional neural mass flow. This attractor is an illustration of the dynamics generated by the flow of a neural mass model (cf. Breakspear et al., 2003). The dynamical variables represent the mean membrane potential of pyramidal (V) and inhibitory (Z) neurons, and the average number of open potassium ion channels (W). (B) Poincaré first return map from the same attractor (Breakspear et al., 2003); this map captures key features of the neural mass flow, by following each trajectory from one intersection (V) of the attractor to the next (P(V)). (C) The quadratic logistic map that has the same unimodal topology as the neural mass Poincaré return map. While the logistic map lacks the "thickness" of the neural mass map, it is several orders of magnitude faster to compute, hence allowing more detailed quantitative analysis. Figure and caption adapted from "Symbiotic relationship between brain structure and dynamics," by. M. Rubinov, O. Sporns, C. van Leeuwen, and M. Breakspear, 2009, *BMC Neuroscience*, *10*(1), 55.

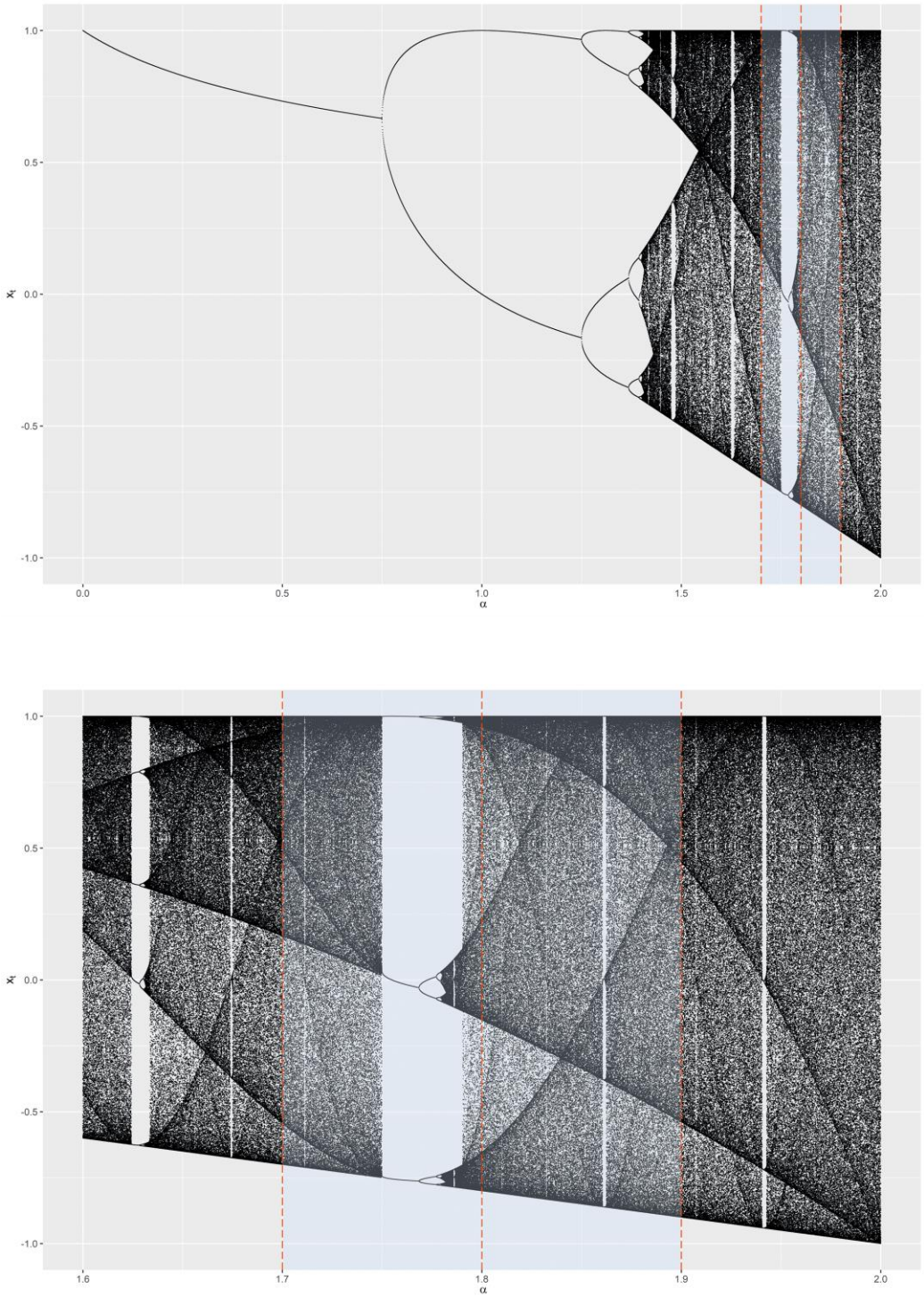

Figure S2. Feigenbaum diagram of the values of the 200 draws of logistic maps (after a burn-in period of 4000 iterations). For three levels of turbulence parameter used in this study (i.e., $\alpha = 1.7, 1.8,$ or 1.9; vertical lines), logistic maps exhibit chaotic behavior hence are suitable dynamic elements in our models.